4th Symposium on Japan-Mexico-USA Consortium for Technological Engineering (JMUCTE). Dec. 2-3 2010, Morelia, Mich., México.

SYNTHESIS AND CHARACTERIZATION OF WO_3 AND WS_2 NANOSTRUCTURES AND CATALYTIC TEST IN SULFUR REMOTION

[1]R. Huirache-Acuña, [2]F. Paraguay-Delgado, [1]M. A. Albiter, [1]J. Lara-Romero, [2]L. Alvarez-Contreras, [3]E. M. Rivera-Muñoz and [4]G. Alonso-Núñez

[1]*Facultad de Ingeniería Química, Universidad Michoacana de San Nicolás de Hidalgo, 58060 Morelia, Michoacán, Mexico.*
[2]*Centro de Investigación en Materiales Avanzados, S. C., Miguel de Cervantes 120, Complejo Industrial Chihuahua, Chih., 31109, Mexico.*
[3]*CFATA-Universidad Nacional Autónoma de México, Boulevard Juriquilla 3001, Juriquilla Querétaro, 76230, Mexico.*
[4]*Centro de Nanociencias y Nanotecnología, Universidad Nacional Autónoma de México, Ensenada, B. C. Mexico.*

rafael_huirache@yahoo.it

Keywords: Nanostructures, hydrothermal, WO_3 and WS_2, sulfur remotion.

INTRODUCTION

Transition metal dichalcogenides TX_2 (T = transition metal of group IVB, VB and VIB, chalcogen, i.e. S, Se and Te) constitute a structurally and chemically well-defined family of compounds [1]. Their uses range from photoactive materials in photoelectrochemical solar cells, to cathodes in solid state lithium batteries, due to their ability to intercalate with lithium ions [1, 2], to lubricants for tribological applications [3], and catalysts [4].

Studies on hydrodesulfurization (HDS) catalysts are nowadays stimulated by the increase in environmental regulations to reduce the amount of sulfur in vehicle transportation fuels [5]. Thus, HDS catalysts are required to be ever more effective. As is well known, a common approach to increase the number of active sites on catalysts is to decrease their particle size to nanostructured materials. For this reason, increasing research has been focused on nanomaterials to be used as HDS catalysts [6]. To date, molybdenum and tungsten sulfides are well known hydrotreating catalysts, used for decades in the treatment of heavy crude oils to eliminate heteroatoms such as sulfur and break-down aromatic molecules [7].
Various strategies have been used for the synthesis of WS_2 nanostructures. For example, WS_2 tubes have been synthesized from $W_{18}O_{49}$ rods produced by heating tungsten foil at high voltages under argon flow in the presence of SiO_2 [8], by the reaction of hexacarbonyl $W(CO)_6$ as precursor with H_2S in argon in a microwave plasma [9], by burning tungsten wire in low-oxygen-partial pressure atmosphere in argon gas [10], and by template self-assembly of anionic tungstates (WS_4^{-2}) and cationic surfactant molecules such as cetyl trimetyl ammonium (CTA^+) in solution under appropriate conditions [11]. Recently, WO_3 was found to be a versatile precursor in the synthesis of nanostructured WS_2 [12, 13]. In this paper we describe the synthesis and characterization of WS_2 nanostructures by using WO_3 in nanostructured form as precursor and a two-step hydrothermal/gas phase reaction method. Additionally, the catalytic properties of this sulfide nanostructure are discussed.

METHODOLOGY

WO_3 nanostructures were synthesized by using a hydrothermal route. For this, a saturated aqueous solution of ammonium metatungstate (0.15 mol of W) was prepared and acidified with HNO_3 2.2 N (pH around 5). It was then kept in a hermetically sealed flask with stirring for 48 h at 333 K. Subsequently, 5 mL of this aged solution were deposited into a Teflon-lined stainless steel autoclave and heated at 473 K for 48 h. The resulting material was filtered, washed and dried at room temperature. To obtain the WS_2 nanostructures, the WO_3 precursor was placed in a tubular reactor and then sulfided for 4 hours under a flow of H_2S/H_2 (15% H_2S) at different temperatures: 673, 773 and 1073 K. The nanostructures were labeled WS_2-673-K, WS_2-773-K, and WS_2-1073-K, according with the temperature set to obtain the material. A Philips microscope model CM200 operated at 200 kV with a LaB_6 filament was used to study the microstructure and elemental composition distribution using the scanning mode (STEM). X-ray diffraction studies were made with a Philips X Pert MPD diffractometer, copper Kα radiation with wavelength λ= 1.54056 Å, operated at 43 kV and 30 mA.

Specific surface area (SSA) was determined with a Quantachrome AUTOSORB-1 model by nitrogen adsorption at 77 K using the BET isotherm. Samples were degassed under flowing argon at 473 K for 2 h before nitrogen adsorption. The HDS of DBT was performed in a 1L volume Parr model 4560 high-pressure batch reactor equipped with magnetically driven turbine. One gram of the WS_2 nanostructures was placed in the reactor with a

solution of 5 vol% of DBT in decaline (total volume 150 mL). The reactor was first purged and then pressurized to 3.1 MPa with hydrogen and heated to 623 K at a rate of 10 K/min, with stirring speed of 600 rpm. After the working temperature was reached, sampling for chromatographic analysis was performed during the course of each run to determine conversion versus time dependence. The reaction was followed for 5 h with sampling of the reaction mixture every 30 minutes.

RESULTS AND DISCUSSION

Owing to the structure of ammonium metatungstate to convert $W_{12}O_{41}^{10-}$ anions to neutral $W_{12}O_{36}$, excess divalent oxygen anions must be removed during the aging of the precursor solution and hydrothermal treating. Stoichiometrically, five divalent oxygen anions per $W_{12}O_{41}^{10-}$ must be combined with protons from the acidic medium:

$$W_{12}O_{41}^{10-} + 10H^+ \rightarrow 12WO_3 + 5H_2O \quad (1)$$

In reaction (1), high concentrations of both $W_{12}O_{41}^{10-}$ and H^+ shift the reaction to the right ensuring the formation of WO_3, although many intermediate steps and thus compounds and phases may exist. The thermal transformation from WO_3 to WS_2 is represented in equations (2) and (3) as follows:

$$WO_3 + H_2 \rightarrow WO_2 + H_2O \quad (2)$$

$$WO_2 + 2H_2S \rightarrow WS_2 + 2H_2O \quad (3)$$

During the sulfidation of tungsten oxide nanoparticles, the first sulfide layer passivates the nanoparticle and prevents coarsening of the nanoparticles into larger platelets. In the next slow step, the partially reduced oxide core is converted into metal-sulfide in a quasi-epitaxial layer by a layer process [14]. It is hypothesized that the hydrogen and oxygen may diffuse through the layers in the radial direction, while sulfur atoms intercalate and diffuse easily along the WS_2 layers until they reach a dislocation, which permits them to diffuse in the radial direction through the layer to the next inner layer [15].

The XRD pattern of the WO_3 nanostructures is presented in Figure 1a and was indexed based on a hexagonal cell for tungsten trioxide (ICSD 32,001, JCPDS 33-1387; a = 7.298 Å, c = 3.899 Å, space group P6/mm) [16]. In this work, we observed that in all cases the intensity peaks for the precursor WO_3 disappear after being treated with H_2S/H_2 at temperatures of 673, 773 and 1073 K, and WS_2 nanostructures were generated. In this study, all diffraction patterns for the 2H-WS_2 phase showed a poor crystalline structure (JCPDS-ICDD 8-237), with a (002) signal at $2\theta \approx 14^\circ$. At this respect, the intensity of the (002) signal is representative of the *"c"* direction layer stacking. The (002) peak for sample WS_2-673-K was higher compared with that presented by the sample WS_2-773-K, and it increased significantly at the highest activation temperature (1073 K). The different intensities of this peak depend on the experimental conditions used in this work and the activation method. As described by Chianelli [17].

Transmission electron microscopy (TEM) micrographs of WO_3 and WS_2 nanostructures at different magnifications are reported in Figures 2a-d. A representative TEM image of the tungsten oxide nanostructures is shown in Figure 2a. The sample consists of not very well separated nanoparticles of rectangular and truncated shape and lengths between 30 to 500 nm and wide from 20 to 90 nm, which aggregated because of the high surface energy due to their nanosize. The HRTEM image of the WO_3 nanostructure shows a lattice distance of 0.39 nm which is very similar to the d-spacing of (001) reported for the WO_3 hexagonal cell.

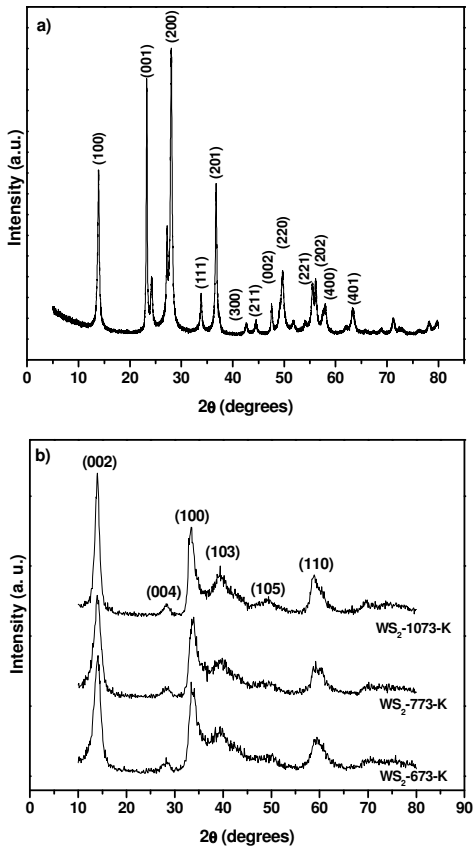

Fig. 1. XRD patterns for: a) WO_3 nanostructure b) WS_2 nanostructures synthesized at different temperatures. Where (002), (004), (100), (105), (103) and (110) represent the planes from 2H-WS_2 structure.

Typical WS_2 fringes (S-W-S layers) were visible on the samples with irregular edges. The inter-planar spacing measured for WS_2 along the "c" direction was ~0.62 nm, which is close to the reported value for (002) planes (0.618 nm). TEM images show a gradual evolution from a smooth surface (WO_3) to a rough material (WS_2)

presenting some hollows as a result of phase change during the sulfidation process.

Table 1. Reaction Rate Constants (k), Specific Surface Area and Selectivity (HYD/DDS) at 5 h of reaction

Sample	k (mol/g*s)	Specific Surface Area (m^2/g)	HYD/DDS
WS_2-673 K	$2.5x10^{-7}$	23	2.32
WS_2-773 K	$3.0x10^{-7}$	29.6	1.75
WS_2-1073 K	$1.6x10^{-7}$	21.9	1.55

The catalytic activity and selectivity (HYD/DDS) at 5 h of reaction for all catalysts are reported in Table 1. A correlation between the SSA and crystal size with the catalytic activity was observed in the present study. A maximum of catalytic activity was observed for the WS_2 nanostructure synthesized at 773 K (k = $3.0x10^{-7}$ mol/g*s, 29.6 m^2/g). This improvement in catalytic activity might be attributed to its slightly larger SSA which could probably expose a higher amount of active sites. In addition, it is probable that this temperature of reduction (773 K) could largely prevent the closure of the structure. This is very desirable since the closed cage structures would only have basal planes exposed to the reactants in the catalytic activity tests, and they are well known to be inactive in HDS reactions [18].

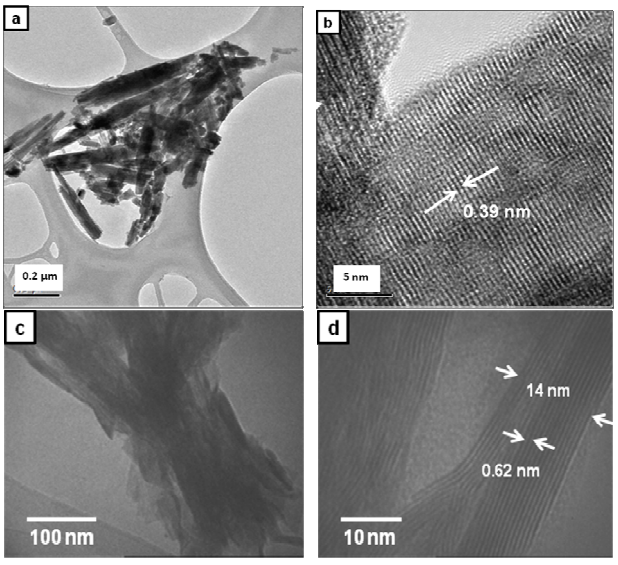

Fig. 2. a) TEM image of tungsten oxide nanostructures, b) HRTEM image of WO_3 nanostructure showing the growth direction, c) y d) TEM images of WS_2 nanostructures synthesized under a flow of H_2S/H_2.

Furthermore, samples WS_2-673-K and WS_2-773-K are more efficient catalysts than *ex situ* single layers of MoS_2 [6]. This enhancement in catalytic activity observed for the presently studied samples with respect to the *ex situ* MoS_2 reference could be related to the morphology and structure change of particles. Since our experimental conditions are close to those used in the industry, we believe that the difference between HYD/DDS ratio is probably due to a difference in the structure of WS_2.

CONCLUSIONS

WS_2 nanostructures with hexagonal phase were successfully obtained using a two-step hydrothermal/gas phase method. Nanostructure morphology was modified after sulfidation of hexagonal WO_3 to 2H-WS_2 catalysts and the sulfidation conditions were found to affect the final morphology, structure and catalytic properties of the WS_2 nanostructures. WS_2-673-K and WS_2-773-K nanostructures were more efficient catalysts than *ex situ* MoS_2 catalyst (non-nanostructured material) evaluated under similar conditions. All samples show a preference for the hydrogenation (HYD) pathway (selectivity).

Acknowledgments

The authors appreciate the valuable technical assistance of C. Ornelas, W. Antúnez, E. Torres (CIMAV, S.C.) and F. Rodriguez-Melgarejo (CINVESTAV-Querétaro). This work was financially supported by CONACYT and postdoctoral scholarship-UNAM.

REFERENCES

1. J. Ouerfelli, S.K Srivastava., J.C. Bernède, S. Belgacem, Vacuum 83, 308-312 (2009).
2. H. Tributsch, Solar Energy Materials Vol. 1, 257-269 (1979).
3. F. Chinas-Castillo, J. Lara-Romero, G. Alonso-Nuñez J.D.O Barceinas-Sánchez and S. Jiménez-Sandoval, Tribology Letters Vol. 26, No. 2, 137-144 (2007).
4. G. Alonso and R.R. Chianelli, J. of Catalysis 221, 657-661(2004).
5. K.G. Knudsen, B. H. Cooper and H. Tøpsoe Appl. Catal. A 89, 205-215 (1999).
6. M. A. Albiter, R. Huirache-Acuña, F. Paraguay-Delgado, J.L. Rico and G. Alonso-Núñez, Nanotechnology 17, 3473-3481(2006).
7. A. Olivas, G. Alonso and S. Fuentes, Topics in Catalysis Vol. 37 Nos. 3-4, 175- 179 (2006).
8. Y. Q. Zhu, W. K. Hsu, N. Grobert, B. H. Chang, M. Terrones, H. Terrones, H. W. Kroto, D.R.M. Walton Chem. Mater. 12, 1190-1194 (2000).
9. D. Vollath, V. Szabó, Materials Letters 35, 236-244, (1998).
10. M. Kurumada, O. Kido, T. Sato, H. Suzuki, Y. Kimura, K. Kamitsuji, Y. Saito, C. Kaito, Journal of Crystal Growth

275, e1673-1678 (2005).
11. Y.D. Li, X.L. Li, R.R. He, J. Zhu and Z. X. Dheng, J. Am. Chem. Soc. Vol. 124 No. 7, 1411-1416 (2002).
12. Tenne R., Margulis L., Genut M., Hodes G. (1992) Nature 360:444-445.
13. R. Huirache-Acuña, F. Paraguay-Delgado, M.A. Albiter, J. Lara-Romero, R. Martínez-Sánchez, Materials Characterization 60, 932-927 (2009).
14. A. Zak, Y. Feldman, V. Alperovich, R. Rosentsveig and R. Tenne, J. Am. Chem. Soc. 122, 11108-11116 (2000).
15. Y. Feldman, G. L. Frey, M. Homyonfer, V. Lyakkhovitskaya, L. Margulis, H. Cohen, G. Hodes, J. L. Hutchison and R. Tenne, J. Am. Chem. Soc. 118, 5362-5367 (1996).
16. H. A. Therese, J. Li, U. Kolb, W. Tremel, Solid State Sciences 7, 67-72 (2005).
17. R. R. Chianelli, International Reviews in Physical Chemistry 2, 127-165 (1982).
18. M. Salmeron, G.A. Somorjai, A. Wold, R. Chianelli, K.S. Liang, Chem. Phys. Lett. 90, 105 (1982).